ShadowTac

Dense Measurement of Shear and Normal Deformation of a Tactile Membrane from Colored Shadows

Vitrani, Giuseppe; Pasquale, Basile; Wiertlewski, Michaël

DOI
10.1109/ICRA55743.2025.11128441

Publication date
2025

Document Version
Final published version

Published in
Proceedings of the IEEE International Conference on Robotics and Automation, ICRA 2025

2025 IEEE International Conference on Robotics and Automation (ICRA)
May 19-23, 2025. Atlanta, USA

ShadowTac: dense measurement of shear and normal deformation of a tactile membrane from colored shadows

Giuseppe Vitrani[1*], Basile Pasquale[2*] and Michaël Wiertlewski[1]

***Abstract*— To robustly handle objects, robots must perceive mechanical interactions through touch with sufficient richness. New tactile sensors leverage miniature cameras to provide dense measurements of these interactions, allowing for the extraction of material properties and frictional information. Among the plethora of solutions, retrographic sensing is popular for its ability to finely resolve the shape of the object being touched. These sensors use a reflective membrane, illuminated at a shallow angle by three RGB lights from which fine details of the surface can be recovered.**

However, these retrographic sensors are unable to detect the lateral displacement of the membrane and, therefore overlook frictional information, which is crucial for grasping and manipulation. Embedding and tracking opaque markers has been a makeshift solution, but these markers occlude the membrane and are difficult to manufacture. In this paper, we introduce ShadowTac, a tactile sensor that combines retrographic illumination with non-intrusive markers created by colored shadows. We patterned the retrographic surface with a dense array of submillimeter dimples, which are small enough not to obstruct the view yet cast shadows large enough to be visible to the camera. ShadowTac captures a dense image of both the normal displacement field with fine details and a precise lateral displacement field by tracking the markers. Additionally, our sensor is easy to manufacture, as the dimple pattern can simply be molded. We evaluated the measurement reliability of ShadowTac and its effectiveness in estimating the incipient slip of arbitrary objects. The dense measurement of both the normal and shear deformation that the sensor captures makes it ideal for tracking dynamic interactions between robotic fingertips and manipulated objects.

I. Introduction

To robustly manipulate unknown objects, robots must understand the mechanical interaction that occurs at the interface. This information is readily available from the sense of touch since extracting tactile cues can inform on the material properties of the object (e.g. friction, softness, shape, textures) and the dynamic state of the contact (e.g. interaction forces, linear and rotational slip). In recent years, vision-based tactile sensors, which use embedded cameras to track the movement of an elastic body, have emerged as promising technologies to capture these tactile cues, as they boast a high resolution in a relatively small package.

These sensors are equipped with a camera, an illumination system, and an elastomeric skin. The latter converts mechanical information into optical data, making surface deformations visible to the camera [1], [2]. The construction of the membrane is fundamental for collecting relevant data. Ideally, the membrane would be built to capture the entire interaction, that is the normal pressure and tangential traction fields that are distributed across the interface between the sensor and the object. If the membrane is soft, these pressure fields induce noticeable normal and tangential deformations that can be captured by a camera.

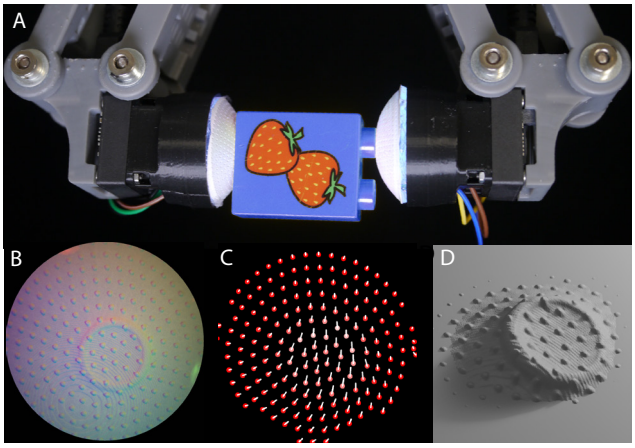

Fig. 1. A. ShadowTac sensors mounted on a gripper. B. Retrographic image with the dimple array. C. Tracked deformation in the normal and tangential direction. D. Reconstructed shape of the indentation.

Having access to the displacement fields at the interface is fundamental for obtaining a complete overview of the contact state, from which tactile cues can be extracted [3], [4]. With sufficiently soft elastomers and high camera resolution, textural features (e.g. screw threads or fingerprints) can be recognized and used, for example, for object classification tasks [5]. However, a dense estimation of both the normal and tangential displacements while maintaining good visibility for superficial features is not trivial to achieve. Most sensors can effectively provide normal or tangential deformation, offering a partial overview of the contact.

The most common technique uses markers embedded in the elastomer to create tactile sensors [6], [7]. The camera is pointed at the marker patterns and tracks their motion in the tangential direction. Although excellent in retrieving lateral information, marker-based methods suffer from low sensitivity when measuring normal displacement, which is important for shape or softness measurement. Stereo vision techniques circumvent this limitation by capturing two viewpoints of the membrane and reconstructing the 3D movement of the markers, at the expense of complex hardware and

[1]Delft University of Technology, Cognitive Robotics Department, 2628 CD, Delft, The Netherlands. g.vitrani@tudelft.nl
[2]École Polytechnique Fédérale de Lausanne, Rte Cantonale, 1015 Lausanne, Switzerland. basilepsqle6@gmail.com
*These authors contributed equally.
Corr. author: Michaël Wiertlewski m.wiertlewski@tudelft.nl
GitHub page: https://github.com/Vitrani/ShadowTac

2025 IEEE International Conference on Robotics and Automation (ICRA) | 979-8-3315-4139-2/25/$31.00 ©2025 IEEE | DOI: 10.1109/ICRA55743.2025.11128441

processing [8], [9]. In addition to lacking normal deformation perception, these sensors struggle to detect surface features due to the sparsity of the markers.

By using the Lambertian reflection of a soft reflective membrane, retrographic sensors achieve pixel-level resolution and can recover a map of the normal deformation. The resolution is high enough to capture detailed features of objects [10]. The membrane is made from a clear elastomer coated with a layer of reflective material, whose inner part is illuminated by a multicolor light pattern, usually 3 RGB LEDs positioned around the membrane at 120° of each other. The deformations of the elastomer create colored patterns that can be decoded using photometric stereo methods to recover the normal deformation. However, because they capture light bouncing off the reflective surface, they cannot detect if the membrane is stretched laterally, and therefore, they are not sensitive to shear.

To add the shear sensitivity to retrographic sensors, it is possible to include opaque markers on the membrane [11], [12]. These markers are either directly painted on the membranes, or made by filling laser-cut holes with dark paint [13]. In both cases, it is challenging to obtain visible and consistent markers below 1 mm in size. It is especially problematic if the sensing surface is curved, which is preferable for robotic grasping and improves the illumination [14]. In addition, since the markers are opaque, they occlude portions of the membrane and hinder the visibility of superficial details. This can be software-corrected but nonetheless undermines one of the main advantages of retrographic sensors [15], [16].

In this article, we propose to solve these limitations with our sensor called ShadowTac (Fig. 1). The sensor can reconstruct the three-dimensional displacement field without suffering from marker occlusions. The sensor uses a single camera and a curved retrographic surface patterned with a dense array of submillimeter dimples illuminated by 3 RGB LEDs. The triplet of shadows generated locally by each dimple is used to track the lateral movement of the skin, while the normal component is retrieved by using photometric stereo. The dimples are unobtrusive enough that the retrographic images can resolve a high level of detail, sufficient to detect small scale features and textures, while maintaining high sensitivity to lateral movements. Achieving similar size and density with traditional markers would present manufacturing challenges, especially on curved surfaces. In contrast, ShadowTac only requires filament-printed components for the sensor casing and an SLA-printed mold to build the membrane, avoiding the use of specialized equipment and making it inexpensive and easy to build. Finally, we show that the dense displacement fields measured by our sensor are repeatable and can be used to continuously estimate the degree of object slippage, which is fundamental to designing real-time delicate grasping algorithms.

II. Related works

A. Marker-based sensors

Marker-based sensors are built around colored markers dispersed in a elastic body. The typical configurations place markers of the same color at the same depth, which implies that algorithms can only recover their lateral movement [17], [18]. The Tactip sensor family [19] uses an array of protruding pins which can tilt and magnify the effect of shear and edge contacts. A similar marker design is used for ViTacTip [20], also featuring a transparent skin to capture objects color.

By positioning the markers at various depths [21], using color changing effects as with the Chromatouch [22], [23], or both [24], the normal component of displacement can also be recovered. However, in most cases, these sensors require a careful alignment of markers [25], challenging manufacturing techniques, and suffer from poor sensitivity.

Finally, stereo vision methods can reconstruct the 3D motion of markers by capturing two images with different points of view. These can be implemented by using either two cameras [26], one camera and mirrors as in Tac3D [8], or a custom stereo vision camera as for the Gelstereo-type sensors [9].

B. Retrographic sensors

The Gelsight [10], [27] represents the earliest retrographic sensing implementation for tactile sensing. Other sensors in this category are directly inspired by Gelsight and focus on improving its technology. For example, the Gelslim family [28] features improved gel durability and smaller size. The ingenious engineering of the DIGIT [29] improves compactness necessary for in-hand manipulation. Other approaches have also mimicked the size and shape of a human finger [30], [31], [32], [33]. Designs such as GelSight360 [34] extend the sensing area by using omnidirectional cameras and custom illumination.

A subset of the retrographic sensors features markers to estimate shear [35] or slip [11], [13]. These sensors are usually flat since adding markers on curved surfaces is challenging. A peculiar implementation is presented in [15], where the markers are only visible under UV light.

III. Design rationale

A. Quantifying shear with curved retrographic sensors

To estimate shear, we track distributed multicolor shadows produced by an RGB light source illuminating a collection of dimples. The movement of these shadows directly correlates with the lateral movement of the reflective membrane. Because the dimples are small (i.e. smaller than 100 microns), we minimize the occlusion of the retrographic membrane, as shown in Fig. 2. The shadows are created by the colored light illuminating a dimple on one side and casting a shadow on the other side. Combining the three color channels generates a stereotypical yellow, cyan, and magenta color pattern around each dimple. The multicolored shadow occupies about 120°, and each shadow is the combination of two light sources with independent wavelengths. The triplet of shadows produced by each color is processed further to determine the lateral motion of the membrane. We design the dimples such that they (1) give uniform local shadows, (2) minimize camera occlusion and (3) support high density on curved surfaces.

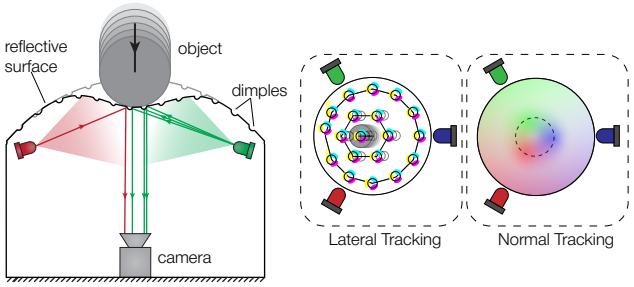

Fig. 2. ShadowTac working principle. Light is emitted around the reflective membrane. The dimple features embedded in the membrane create distinctive shadows from which the lateral displacement can be tracked. Retrographic methods can reconstruct the normal displacement field.

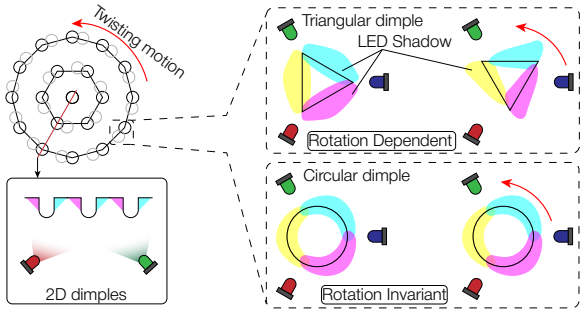

Fig. 3. Comparison of two dimple shapes. Sharp edges generate inconsistent shadows. Instead, symmetric structures eliminate distortions and provide larger shadows.

Making the shadows uniform across the membrane affects directly the robustness of the lateral tracking pipeline. To minimize discrepancies, we carefully choose the shape and size of the dimples. In fact, the illumination of each dimple was chosen so it remains uniform when the membrane undergoes large deformations.

While designing, we need to compromise between having dimples as small as possible to avoid occlusion of the retrographic membrane and as large as possible to cast shadows that are detectable by the camera. A satisfactory tradeoff is achieved for 1 mm dimples or smaller in width. At this scale, the recognition of surface features is preserved even if the density of dimples is high. Reaching a similar density and size with traditional opaque markers is challenging.

B. How dimple shape affects shadows

The chosen shape of each dimple is critical for a correct shadowing effect and, by extension, for the proper behavior of the tracking pipeline of the ShadowTac. In particular, when the membrane twists, it can cause illumination problems since it induces a rotation of the dimples (see Fig. 3). If the dimples have a shape with sharp edges, as is the case of tetrahedrons, the shadow will change upon rotation since each edge will receive a different amount of light. Instead, axisymmetric structures such as hemispheres produce rotation-invariant shadow profiles, which are suited for tracking complex motions.

However simple hemispheres are not trivial to design, since to reduce the view occlusion, hemispheric dimples must have small radii, but they generate small shadows. Worse, the small dimples have shadows that tend to disappear under small forces due to their insufficient height. As a result, we found that dimples with a cylindrical shape and hemispheric tip solve both issues. Their height is adjustable as desired, thus improving the shadow formation, and their symmetry makes rotation invariant shadows. Moreover, they can be small enough to reduce occlusion.

IV. Manufacturing

A. Sensing skin

The material used for the fabrication of the sensing skin is chosen to be fully transparent, soft to enable delicate object handling, and durable to avoid wear after extensive use. Hence, we chose the Smooth-On Solaris with a shore hardness of 15A and further softened by adding 40% Smooth-On Silicone Thinner.

We designed the mold to cast a hemispherical skin with a diameter of 35 mm and a height of 8 mm. After multiple design iterations, we defined the height and base of the dimples to be 0.5 mm and 0.45 mm, respectively. We arranged them concentrically on the silicone with a spacing of 1.4 mm, resulting in 200 detectable markers in total. The mold was first sprayed with a mold release product, and then the silicone was poured into the mold, degassed, and left to cure for 24 hours.

After demolding, a thin reflective layer was brushed to the dimple-engraved silicone. The paint consists of Smooth-On PsychoPaint mixed with aluminum powder, Silc Pig white pigment to increase opacity and reduce external light interference, and a silicone solvent. Finally, the painted silicone was glued to a supporting PMMA acrylic plate using Smooth-On SilPoxy glue. The procedure to fabricate the sensor is shown in Fig. 4.

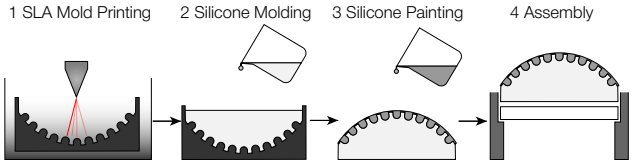

Fig. 4. Sensor manufacturing procedure. The mold is first created, then the silicone membrane is cast. Once the membrane is unmolded, we paint the reflective layer and assemble it to the sensor body.

B. Illumination, camera and assembly

The illumination consists of three RGB LEDs cut from a Mini Skinny NeoPixel RGB strip. They feature a large emission angle, are low-power and individually controllable. The red, blue, and green lights are evenly spaced and positioned at an angle of 120°, close to the acrylic plate to avoid spurious reflections.

We use a Basler daA1920-160uc (S-Mount) camera mounted with the Evetar Lens M13B02820W. The wide-angle lens has a small focal length, suitable to be placed

close to the acrylic plate, which is glued to the case by using cyanoacrylate glue. The casing consists of two filament-printed components: one that supports the camera, LEDs, and sensing membrane, while the other is a base to mount the sensor on a robotic gripper. An exploded view of the ShadowTac is visible in Fig. 5.

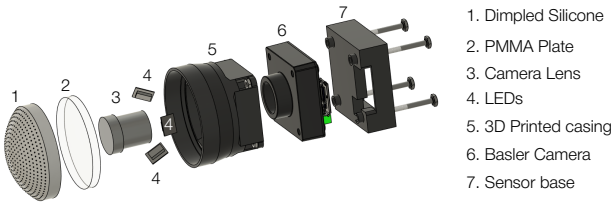

Fig. 5. Exploded view of the ShadowTac sensor. The silicone membrane and the camera are mounted in a plastic housing.

V. Tactile Image Processing

The reconstruction of normal and tangential information requires two separated pipelines.

First, the normal component (Fig. 6(A)) is obtained using a photometric stereo algorithm [36], commonly used in retrographic sensors. This algorithm calculates a normal map, which is then used to generate a depth (or height) map that provides the normal component for each pixel. To reveal details of the objects, the height map is calculated over the entire tactile image minus the initial dome height. Instead, for dynamic events, we improve computation speed by subsampling the raw image for height calculation and evaluating the depth at the dimple positions. An experimental scaling factor is applied to convert pixels to millimeters.

Second, to track the lateral motion of our dimples, we use the processing pipeline shown in Fig. 6(B). The tactile image is first separated into red, green, and blue color channels. Then, each of these channels is shifted by a few pixels in the direction of its corresponding LED. This operation overlaps the three colored shadows into a single dark spot centered at the location of the respective dimple. At this stage, the image can be converted into HSV format and then binarized using an adaptive threshold. Finally, the centroids of each marker are detected using a blob detection method, and another scaling factor is applied to convert pixels to millimeters.

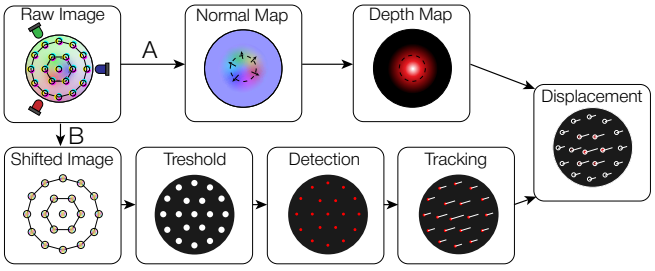

Fig. 6. Image processing pipeline for the normal (A) and lateral (B) movement of the soft silicone membrane.

Sudden contacts can cause random shadows to disappear and consequently cause errors in the estimation of their lateral position. To mitigate this effect, we further robustify their tracking. For each frame, we associate each marker with its previous position if their relative distance is smaller than a specified threshold. If there are markers from the previous frame that are not matched with any in the current frame, a local displacement is calculated by using its nearest neighbors, which ensures a consistent number of detected markers and simplifies computations such as slippage estimation.

VI. Setup and Data Acquisition

We collected a dataset to evaluate the repeatability of our sensor and another dataset to test its ability to estimate tangential slip. The setup we used to capture the data is shown in Fig. 7(A). It is built around two motorized linear stages (Thorlabs NRT150/M) and a FT force sensor (ATI Nano 43). It lowers one of three 3D-printed objects onto the sensor. We used two spheres and one cylinder with diameters 20, 50 and 40 mm respectively. The objects used were positioned at the center of the elastomeric skin at the beginning of every trial. The tactile images and normal and lateral forces were acquired at a frequency of 5 Hz, with careful synchronization between the images and forces.

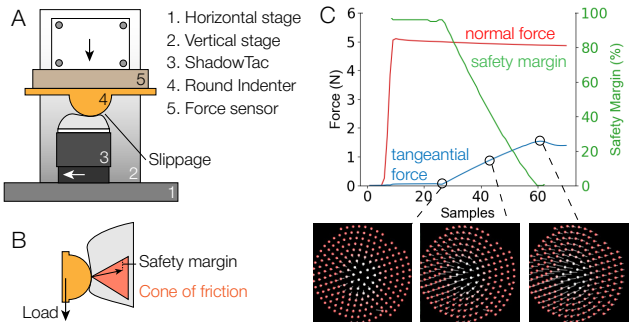

Fig. 7. A. View of the setup used for data acquisition. B. The safety margin represents the amount of lateral force before the object starts slipping. C. Example of sliding test: the data shows the acquired forces and the calculated safety margin, along with the sensed displacement field.

To measure how far from slip an object is, we calculate the so-called *safety margin* (Γ), which was previously used in [4]. It assesses the degree of partial slip and can be directly used to regulate grasping forces. Γ is the amount of lateral force that would push the object outside the frictional limit and make it slip, as shown in Fig. 7(B). It is defined as $\Gamma = \frac{F_t^* - F_t}{F_t^*}$, where F_t^* is the critical tangential force for a given object when full slippage occurs (i.e. macroscopic relative movement between sensor and object) and F_t is the current one. Γ was calculated from the recorded lateral forces, with F_t^* defined as the maximum value reached in each sliding trial. Γ ranges from 0 (gross slippage reached and object sliding away from grasp) to 100% (no tangential forces applied). When Γ is between 0 and 100%, the contact is partially slipping, where some regions are stuck and others are slipping.

During the acquisition of the slippage dataset (see an example in Fig. 7(C)), an indenter was first vertically pressed on the ShadowTac, then laterally displaced with a velocity of 0.15 mm/s until full slippage was reached. In specific trials, we modified the frictional properties by wetting the contact surface with water. We conducted 14 sliding experiments:

- cylinder: indentations of 1, 2, 3 mm; 2, 3mm wet.
- 50mm sphere: indentations of 2, 3, 4mm; 3mm wet.
- 20mm sphere: indentations of 2, 3, 4mm; 3, 4mm wet.

In this dataset, we considered normal forces up to 6 N, and the friction coefficient varied from about 0.35 for dry surfaces to 0.25 for wet ones. The sliding direction was the same for all the trials, however, to simulate multiple directions of slippage, the original dataset was rotated six times considering a spacing of 60° (i.e. from 0° to 360°).

For the repeatability dataset, we used the spherical indenter with a diameter of 20 mm and performed the following two experiments, executed 8 times, first with a normal indentation up to 3 mm at a velocity of 0.1 mm/s. No lateral displacement was considered. Followed by a normal indentation of 3 mm followed by a lateral displacement at a velocity of 0.1 mm/s. We considered only the data before the full slip was detected.

VII. Results

A. Occlusion reduction

We assessed the advantage of our dimple design when compared to standard opaque markers by reconstructing the shape of the same object with the two approaches.

We pressed a spur gear on our sensor and generated a 3D reconstruction of the contact surface using the height map computed from the photometric stereo algorithm (Fig. 8A). Next, we simulated black markers at each dimple position, with a width of 0.5mm in (B) and 0.7mm in (C), which is smaller than the state of the art. Finally, we computed the full 3D reconstruction. Although the dimples were still visible in the height map, they conformed to the gear geometry, leaving a high precision of the contour. In contrast, the opacity of the black markers created non-physical flat regions on the height map, completely lacking local shape information.

Black markers also affected the global intensity of the height map, for an unclear reason. Fig. 8(D) shows the height map cross-section for the case with dimples or with dark markers. The height maps generated with dark markers show lower values compared to those with dimples. Specifically, the 0.5 mm markers reduced the maximum computed height by 12% relative to the dimples, while the 0.7 mm markers caused a reduction of 20%. One possible explanation is that the dark markers absorb most of the light that illuminates the membrane, resulting in an overall reduction of the reflected light available for the photometric stereo computations.

B. Displacement repeatability

We evaluated how repeatable the computed displacement fields are when our sensor is pressed on an object. The repeatability test is crucial to assess whether the dimples create consistent shadows during both the indentation and sliding phases when interacting with the same object.

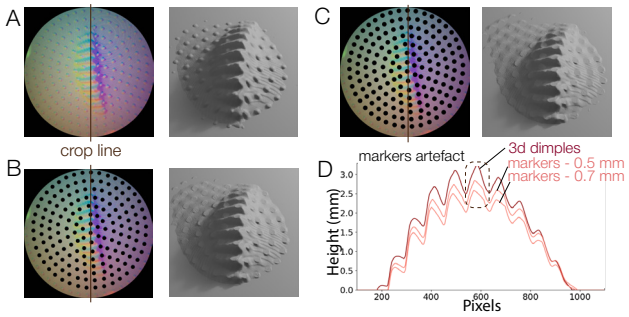

Fig. 8. Sensor images and 3D reconstructions of a spur gear pressed on the sensor. A. Shadowtac dimples. B. 0.5 mm dark markers. C. 0.7 mm dark markers. D. Comparison of cross-section height maps.

Fig. 9 shows a clear linear trend between the average displacement field and the force for both the normal and tangential case. Specifically, a linear fit gives a mean absolute error of 1.4×10^{-3} mm and R^2 of 0.997 for the normal displacement, and a mean absolute error of 1.85×10^{-2} mm and R^2 of 0.988 for the lateral one. These results show the consistency of the sensor behavior when subjected to the same indentation modality.

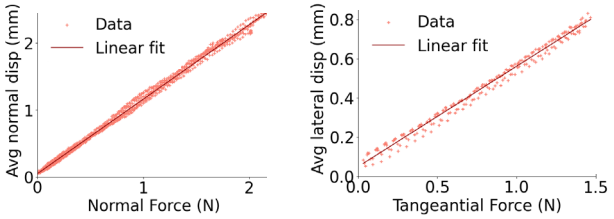

Fig. 9. Repeatability test for normal and tangential displacements when the sensor is pressed with a spherical object.

The sensor could detect a minimal displacement of 0.05 mm normally and 0.5 mm tangentially, based on noise level analysis at rest.

C. Slip degree estimation

A schematic of the Γ estimation pipeline is shown in Fig. 10(A). The tactile images, processed as in section V, produce a 3D displacement field that was used as input to a Multi-Layer Perceptron (MLP). The input dimension is the number of sensor markers multiplied by the number of coordinates, which is in the order of 600 depending on the specific skin. The network included three hidden layers with 256, 128, and 32 units, all using the ReLU activation function. The output layer had 1 unit with Sigmoid activation to constrain the Γ predictions between 0 and 1. The update frequency reached 10 Hz on the CPU (Intel Xeon(R) W-2223 CPU @ 3.60GHzx8).

The trial with the dry 50 mm sphere indented 3 mm was set aside from the entire dataset. The model was trained using data split for the remaining 13 trials: 20% of the slip dataset was reserved for testing, while the remaining 80% was divided into 80% for training and 20% for validation. We used mean absolute error as a loss function and an *Adam*

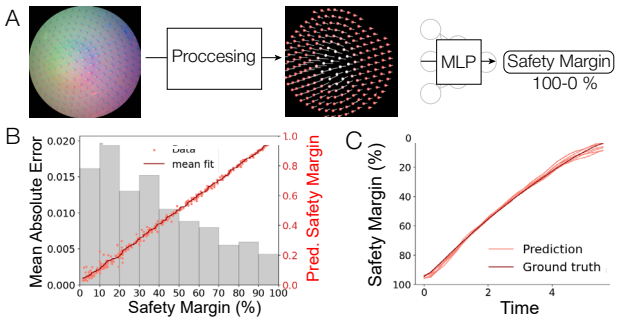

Fig. 10. A. Slip degree estimation pipeline. The image is processed to find the 3d deformation field, which is used by a simple neural net to estimate the safety margin. B. Performance of the slip estimation on the test dataset. C. Performance of the slip estimation for dry 50 mm sphere, which was unseen during training.

optimizer: after 400 epochs, train and validation loss converged to 0.011 and 0.016, respectively. Given the shallow MLP architecture, the training time was about 2 minutes on a regular CPU laptop (Intel i7-9750H @ 2.60GHz).

Fig. 10(B) shows the predicted versus measured Γ for the test dataset, demonstrating high estimation accuracy with an average mean absolute error of 0.014. The gray bargraph represents the mean absolute error for 10% variation of Γ. The mean absolute error is slightly higher when Γ decreases, which is expected since conditions close to full slippage are more challenging to predict.

Finally, Fig. 10(C) shows the predicted versus the measured Γ (ground truth) for the dry 50 mm sphere indented 3 mm, which was an unseen condition during the training. The results show that the network is able to match to a high degree the ground truth, even for data it has not seen before. We predicted Γ for the six rotated versions of the dataset to evaluate the ability of the model to predict slippage in different directions. The model maintains high accuracy, with a mean absolute error of 0.014, averaged across all directions.

VIII. Discussion and Conclusion

We introduced ShadowTac, a retrographic sensor that provides dense 3D deformation measurements and detailed contact features. It achieves these features by tracking markers made from colored shadows. The shadows are generated by the interaction of the RGB illumination with submillimetric dimples of the reflective membrane. These dimples are obtained by simply casting the silicone in an SLA mold, bypassing the tedious process of adding black markers through laser cutting or manual painting. ShadowTac robustly implements the retrographic reconstruction and avoids the interference that opaque markers usually create.

We assessed the advantages of dimples compared to black dots, which were artificially added in the same positions as the real dimples in the image. Although the dimples remain visible in the resulting height map, they tend to conform to local features qualitatively better than the marker array. Since the dimples cast a clearly identifiable pattern of colored shadows on the retrographic image, we can envision an algorithm to remove their influence and completely filter them out from the height map reconstruction. Conversely, opaque markers generate non-physical flat regions that completely remove the local information about shape, making it impossible to reconstruct the actual height map.

The sensor outputs highly consistent values when subjected to repeated measurements. This consistency clearly indicates the stability of the shadows pattern upon deformation of the membrane.

Finally, this sensor is suitable for predicting dynamic events, such as the transition from stick to slip for objects with unknown geometries and frictional properties. Previous works such as [11], [13] only registered signals after the object is fully slipping, which might be too late for grip force regulation of delicate objects. Instead, using the safety margin Γ, we continuously inform the controller about how close the tangential force is to the frictional limit, ensuring that we apply the minimal grip force while maintaining a safe grasp. To estimate Γ, we fed the displacement of 200 markers into a basic multi-layer perception. A previous attempt using the Chromatouch sensor with 4 times fewer markers required a Convolutional Neural Network (CNN) to compute Γ from the entire tactile image [4]. This complex network compensated for the poor measurement density by processing the full images. Instead, our approach uses a dense displacement and is more suited to be processed by simple models, as the sensor extracts meaningful data that strongly correlates with the interaction at the contact and dynamic events such as partial slip.

While the results are promising, further evaluation in less controlled environments is necessary. It is unclear if the model can generalize to a wide range of unseen objects, and we need to assess how effective the slip sensing is when sliding in an arbitrary direction since it was tested on artificially rotated data. Improvements to the Γ prediction pipeline are needed to increase the sampling frequency (limited to 10 Hz) and enable robust real-time control.

Future research will focus on improving the shape and size of the dimples to enhance the robustness of shadow generation under complex loading conditions. We will design an algorithm to filter out the disturbances that the dimples produce during the normal reconstruction. We plan to implement our sensor on a robotic gripper to test its ability to predict linear and rotational slip and other dynamic events. Improving the frequency of estimation of the slip degree, for example by enhancing the image processing pipelines, will in turn improve the control performance for delicate grasping.

IX. Acknowledgments

The authors thank Lukas Stracovsky, Mostafa Atalla and Herbert Shea for their valuable insights. GV and MW acknowledge the support of the Vidi project 19680 financed by the Dutch Research Council (NWO).

References

[1] K. Kamiyama, H. Kajimoto, N. Kawakami, and S. Tachi, "Evaluation of a vision-based tactile sensor," in *IEEE International Conference on Robotics and Automation, 2004. Proceedings. ICRA'04. 2004*, vol. 2. IEEE, 2004, pp. 1542–1547.

[2] S. Zhang, Z. Chen, Y. Gao, W. Wan, J. Shan, H. Xue, F. Sun, Y. Yang, and B. Fang, "Hardware technology of vision-based tactile sensor: A review," *IEEE Sensors Journal*, vol. 22, no. 22, pp. 21 410–21 427, 2022.

[3] W. Yuan, C. Zhu, A. Owens, M. A. Srinivasan, and E. H. Adelson, "Shape-independent hardness estimation using deep learning and a gelsight tactile sensor," in *2017 IEEE International Conference on Robotics and Automation (ICRA)*. IEEE, 2017, pp. 951–958.

[4] D.-J. Boonstra, L. Willemet, J. Luijkx, and M. Wiertlewski, "Learning to estimate incipient slip with tactile sensing to gently grasp objects," in *2024 IEEE International Conference on Robotics and Automation (ICRA)*. IEEE, 2024, pp. 16 118–16 124.

[5] R. Li and E. H. Adelson, "Sensing and recognizing surface textures using a gelsight sensor," in *Proceedings of the IEEE Conference on Computer Vision and Pattern Recognition*, 2013, pp. 1241–1247.

[6] K. Kamiyama, K. Vlack, T. Mizota, H. Kajimoto, K. Kawakami, and S. Tachi, "Vision-based sensor for real-time measuring of surface traction fields," *IEEE Computer Graphics and Applications*, vol. 25, no. 1, pp. 68–75, 2005.

[7] M. Li, T. Li, and Y. Jiang, "Marker displacement method used in vision-based tactile sensors—from 2-d to 3-d: A review," *IEEE Sensors Journal*, vol. 23, no. 8, pp. 8042–8059, 2023.

[8] L. Zhang, Y. Wang, and Y. Jiang, "Tac3d: A novel vision-based tactile sensor for measuring forces distribution and estimating friction coefficient distribution," *arXiv preprint arXiv:2202.06211*, 2022.

[9] C. Zhang, S. Cui, S. Wang, J. Hu, Y. Huangfu, and B. Zhang, "High-precision 3d reconstruction study with emphasis on refractive calibration of gelstereo-type sensors," *Sensors*, vol. 23, no. 5, p. 2675, 2023.

[10] M. K. Johnson and E. H. Adelson, "Retrographic sensing for the measurement of surface texture and shape," in *2009 IEEE Conference on Computer Vision and Pattern Recognition*. IEEE, 2009, pp. 1070–1077.

[11] S. Dong, W. Yuan, and E. H. Adelson, "Improved gelsight tactile sensor for measuring geometry and slip," in *2017 IEEE/RSJ International Conference on Intelligent Robots and Systems (IROS)*. IEEE, 2017, pp. 137–144.

[12] D. Ma, E. Donlon, S. Dong, and A. Rodriguez, "Dense tactile force estimation using gelslim and inverse fem," in *2019 International Conference on Robotics and Automation (ICRA)*. IEEE, 2019, pp. 5418–5424.

[13] I. H. Taylor, S. Dong, and A. Rodriguez, "Gelslim 3.0: High-resolution measurement of shape, force and slip in a compact tactile-sensing finger," in *2022 International Conference on Robotics and Automation (ICRA)*. IEEE, 2022, pp. 10 781–10 787.

[14] S. Wang, Y. She, B. Romero, and E. Adelson, "Gelsight wedge: Measuring high-resolution 3d contact geometry with a compact robot finger," in *2021 IEEE International Conference on Robotics and Automation (ICRA)*. IEEE, 2021, pp. 6468–6475.

[15] W. Kim, W. D. Kim, J.-J. Kim, C.-H. Kim, and J. Kim, "Uvtac: Switchable uv marker-based tactile sensing finger for effective force estimation and object localization," *IEEE Robotics and Automation Letters*, vol. 7, no. 3, pp. 6036–6043, 2022.

[16] N. Ou, Z. Chen, and S. Luo, "Marker or markerless? mode-switchable optical tactile sensing for diverse robot tasks," *arXiv preprint arXiv:2408.08276*, 2024.

[17] A. Yamaguchi and C. G. Atkeson, "Implementing tactile behaviors using fingervision," in *2017 IEEE-RAS 17th International Conference on Humanoid Robotics (Humanoids)*. IEEE, 2017, pp. 241–248.

[18] G. Obinata, A. Dutta, N. Watanabe, and N. Moriyama, "Vision based tactile sensor using transparent elastic fingertip for dexterous handling," in *Mobile Robots: Perception & Navigation*. IntechOpen, 2007.

[19] B. Ward-Cherrier, N. Pestell, L. Cramphorn, B. Winstone, M. E. Giannaccini, J. Rossiter, and N. F. Lepora, "The tactip family: Soft optical tactile sensors with 3d-printed biomimetic morphologies," *Soft robotics*, vol. 5, no. 2, pp. 216–227, 2018.

[20] W. Fan, H. Li, W. Si, S. Luo, N. Lepora, and D. Zhang, "Vitactip: Design and verification of a novel biomimetic physical vision-tactile fusion sensor," *arXiv preprint arXiv:2402.00199*, 2024.

[21] C. Sferrazza and R. D'Andrea, "Design, motivation and evaluation of a full-resolution optical tactile sensor," *Sensors*, vol. 19, no. 4, p. 928, 2019.

[22] X. Lin and M. Wiertlewski, "Sensing the frictional state of a robotic skin via subtractive color mixing," *IEEE Robotics and Automation Letters*, vol. 4, no. 3, pp. 2386–2392, 2019.

[23] R. B. Scharff, D.-J. Boonstra, L. Willemet, X. Lin, and M. Wiertlewski, "Rapid manufacturing of color-based hemispherical soft tactile fingertips," in *2022 IEEE 5th International Conference on Soft Robotics (RoboSoft)*. IEEE, 2022, pp. 896–902.

[24] K. Sato, K. Kamiyama, N. Kawakami, and S. Tachi, "Finger-shaped gelforce: sensor for measuring surface traction fields for robotic hand," *IEEE Transactions on Haptics*, vol. 3, no. 1, pp. 37–47, 2009.

[25] X. Lin, L. Willemet, A. Bailleul, and M. Wiertlewski, "Curvature sensing with a spherical tactile sensor using the color-interference of a marker array," in *2020 IEEE International Conference on Robotics and Automation (ICRA)*. IEEE, 2020, pp. 603–609.

[26] T. Zhang, Y. Cong, X. Li, and Y. Peng, "Robot tactile sensing: Vision based tactile sensor for force perception," in *2018 IEEE 8th Annual International Conference on CYBER Technology in Automation, Control, and Intelligent Systems (CYBER)*. IEEE, 2018, pp. 1360–1365.

[27] W. Yuan, S. Dong, and E. H. Adelson, "Gelsight: High-resolution robot tactile sensors for estimating geometry and force," *Sensors*, vol. 17, no. 12, p. 2762, 2017.

[28] E. Donlon, S. Dong, M. Liu, J. Li, E. Adelson, and A. Rodriguez, "Gelslim: A high-resolution, compact, robust, and calibrated tactile-sensing finger," in *2018 IEEE/RSJ International Conference on Intelligent Robots and Systems (IROS)*. IEEE, 2018, pp. 1927–1934.

[29] M. Lambeta, P.-W. Chou, S. Tian, B. Yang, B. Maloon, V. R. Most, D. Stroud, R. Santos, A. Byagowi, G. Kammerer, *et al.*, "Digit: A novel design for a low-cost compact high-resolution tactile sensor with application to in-hand manipulation," *IEEE Robotics and Automation Letters*, vol. 5, no. 3, pp. 3838–3845, 2020.

[30] J. Zhao and E. H. Adelson, "Gelsight svelte: A human finger-shaped single-camera tactile robot finger with large sensing coverage and proprioceptive sensing," in *2023 IEEE/RSJ International Conference on Intelligent Robots and Systems (IROS)*. IEEE, 2023, pp. 8979–8984.

[31] H. Sun, K. J. Kuchenbecker, and G. Martius, "A soft thumb-sized vision-based sensor with accurate all-round force perception," *Nature Machine Intelligence*, vol. 4, no. 2, pp. 135–145, 2022.

[32] D. F. Gomes, Z. Lin, and S. Luo, "Geltip: A finger-shaped optical tactile sensor for robotic manipulation," in *2020 IEEE/RSJ International Conference on Intelligent Robots and Systems (IROS)*. IEEE, 2020, pp. 9903–9909.

[33] Z. Lin, J. Zhuang, Y. Li, X. Wu, S. Luo, D. F. Gomes, F. Huang, and Z. Yang, "Gelfinger: A novel visual-tactile sensor with multi-angle tactile image stitching," *IEEE Robotics and Automation Letters*, 2023.

[34] M. H. Tippur and E. H. Adelson, "Gelsight360: An omnidirectional camera-based tactile sensor for dexterous robotic manipulation," in *2023 IEEE International Conference on Soft Robotics (RoboSoft)*. IEEE, 2023, pp. 1–8.

[35] W. Yuan, R. Li, M. A. Srinivasan, and E. H. Adelson, "Measurement of shear and slip with a gelsight tactile sensor," in *2015 IEEE International Conference on Robotics and Automation (ICRA)*. IEEE, 2015, pp. 304–311.

[36] R. J. Woodham, "Photometric method for determining surface orientation from multiple images," *Optical engineering*, vol. 19, no. 1, pp. 139–144, 1980.